Proceedings of the 2013 IEEE International Electric Machines and Drives Conference (IEMDC)

Chicago, Illlinois
USA

May 12–15, 2013

Technical Co-Sponsors

IEEE Industry Applications Society (IAS)
IEEE Industrial Electronics Society (IES)
IEEE Power and Energy Society (PES)
IEEE Power Electronics Society (PELS)

http://www.iemdc2013.org

Permanent Magnet Synchronous Reluctance Machine - bridge design for two-layer applications

S. Rick, M. Felden, M. Hombitzer and K. Hameyer
Institute of Electrical Machines
RWTH Aachen University
Email: sebastian.rick@iem.rwth-aachen.de

***Abstract*—The permanent magnet synchronous reluctance machine (PMSynRM) is a combination of the characteristics of two machine types: High efficiency, high power density of the permanent magnet synchronous machine (PMSM) as well as better high-speed performance and lower costs of the synchronous reluctance machine (SynRM). This paper presents a general approach for the electro-magnetic design of a PMSynRM. Essential design rules for constructing a PMSynRM are shown. In particular the rotor configuration is improved by dimensioning of the bridges between flux barriers and air gap. An interior permanent magnet synchronous machine (IPMSM) with two layers which form the flux barriers in the rotor is used as reference. The results are concluded in an objective function.**

***Index Terms*—Bridge, permanent magnet machine, synchronous reluctance, torque.**

I. Introduction

This paper concerns the design of a permanent magnet synchronous reluctance machine (PMSynRM), especially the constellation of different bridge dimensions in an interior permanent magnet synchronous machine (IPMSM) with a flux barrier consisting of two layers. The principle of a PMSynRM can be described as the superposition of two different machine types, the permanent magnet synchronous machine (PMSM) and the synchronous reluctance machine (SynRM). The aim of this design is to benefit of the advantages of both machine types. On the one hand the PMSM provides high efficiency and power density as a result of the use of high energy rare-earth magnets [1]. On the other hand the SynRM is more robust, has lower costs and allows a higher speed level. The PMSynRM is designed for a better utilization of reluctance torque in IPMSMs. The presented results are based on numerical simulations (FEA).

A main difficulty for designing a PMSynRM is to combine all relevant design aspects for an optimal efficiency of the machine, but not to overstress the count of parameter variations and thereby the capacity of the simulation processing system. Many possible parameters are coupled to each other, what causes a huge amount of parameter variations that have to be taken into account. One widely applied approach is to focus on some parameters and simplify the remaining ones. This results in an simplified design than varying every parameter, but has a much shorter calculation time. For this reason in this paper different variations of the bridges in the rotor geometry are compared and integrated in an objective function, which describes a beneficial constellation of bridge widths of a PMSynRM. The advantage of this procedure is a better design result with lower computational costs. The objective function will be derived from electro-magnetic and mechanical point of view. Therefore it depends on the maximum achievable torque by improving the flux path in the magnetic circuit and the maximum reachable speed for ensuring mechanical resistance and stability of the machine. A small bridge width reduces the stray flux in the rotor, but also reduces the stability and thus the reachable maximum speed of the machine [2],[3]. Large bridge widths result in higher stability, which enables higher maximum speed. In this case the stray flux gets higher and the resulting total torque decreases [4]. This paper presents a method to find a beneficial compromise for speed and torque by designing the bridges. To analyze only the effect of different bridge widths a model of the PMSynRM with two layers has been chosen. Based on this model different improvements of the geometry are tested to analyze their influence on the magnetic circuit. By using a two-layer application, the bridge width of the first and the second barrier are changed independently. For every configuration the synchronous and reluctance torque is calculated for an operating point in the base speed range. In a second simulation process the stability is calculated by analyzing the maximum stress for the bridges according to the maximum speed of the machine.

To achieve high power density in the presented machine it is very important to adjust the thickness of the bridges at the end of each barrier. The thickness of the bridges is adapted to the position, the thickness of the barriers and the dimensions of the corresponding permanent magnets. Many of these designing parameters are coupled to each other, which results in an individual simulation analysis. A guideline for the design of the barrier shape is given. The influences of variations in magnet height and width as well as different remanence inductions for the magnets are discussed. A variation of air gap width is performed. The objective function results in a maximum design factor dependent on the obtained constellation of bridge widths. The derivation of this design factor and the handled challenges in simulation and interpretation of the results are described. A better machine design or lower calculation costs can be achieved by the preselection of beneficial bridge width constellations.

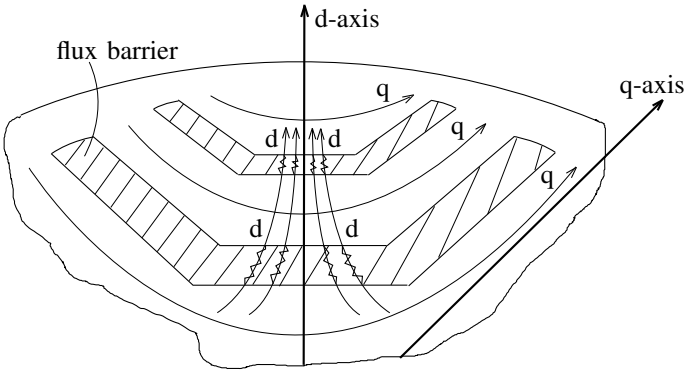

Figure 1. Flux path in the PMSynRM: d- and q-component of magnetic flux in a two-layer rotor geometry. Barriers are in shaded area. No differention between magnet material and air. Blocking the d-flux by the barriers is shown.

II. Electro-magnetic design of the rotor geometry by d-q-transformation

In this section the electro-magnetic design of a PMSynRM is presented. It consists of a fundamental approach to evaluate synchronous- and reluctance torque in a PMSynRM (A), followed by an analysis of a parameterized rotor model (B). Afterward different design rules concerning the magnetic circuit are applied (C).

A. Torque calculation in the PMSynRM

The torque M produced in a PMSM with buried magnets can be divided in two parts in general, the synchronous torque M_{syn} and the reluctance torque M_{rel}. The synchronous torque M_{syn} is proportional to the flux of the permanent magnets Ψ_{PM} and therefrom dependent on the magnet material. Considered properties of the permanent magnets are remanence induction B_{r}, magnet height h_{m} and magnet width w_{m}. A remanence induction $B_{\mathrm{r}} = 0.8\,\mathrm{T}$ is assumed for all calculations except the analysis of varying the remanence induction. Reluctance torque M_{rel} is generated from magnetic preferred directions in the geometry of the rotor, the so-called saliency [5],[6]. In use of d- and q-transformation the total torque can be described by

$$M = p \cdot (\underbrace{\Psi_{\mathrm{PM}} \cdot i_{\mathrm{q}}}_{M_{\mathrm{syn}}} + \underbrace{(L_{\mathrm{d}} - L_{\mathrm{q}}) \cdot i_{\mathrm{d}} \cdot i_{\mathrm{q}}}_{M_{\mathrm{rel}}}) \qquad (1)$$

with the correspondent dq-transformed components of the stator current i_{d} and i_{q} [7]. It is necessary to maximize the difference between d-inductance L_{d} and q-inductance L_{q} to reach the maximum reluctance torque [8].

The flux barriers are constructed in such an extent that the flux is guided in the desired way. The d-axis respectively the q-axis is indicated in Fig. 1. The d-flux is blocked by the two barriers of one pole and the q-flux is guided across an iron path in the rotor [9]. High reluctance of air and magnet material causes a low magnetic conductivity and therefore a smaller d-inductance L_{d}. Higher proportion of reluctance torque allows higher torque density or less synchronous torque to reach the same total torque. In this case lower priced magnets with lower remanence induction are applicable.

Table I
Parameters for machine design.

symbol	quantity	unit	description
k	-	W	design factor
B_{r}	0.8	T	remanence induction
d_1	0.2 to 2.0	mm	bridge width barrier 1
d_2	0.2 to 2.0	mm	bridge width barrier 2
M	-	Nm	torque
M_{syn}	-	Nm	synchronous torque
M_{rel}	-	Nm	reluctance torque
p	2	-	pole pairs
Ψ_{PM}	-	Wb	permanent magnet flux linkage
L_{d}	-	H	d-inductance
L_{q}	-	H	q-inductance
i_{d}	-	A	d-current
i_{q}	-	A	q-current
R_{m}	-	A/Wb	reluctance
μ_0	$4\pi 10^{-7}$	N/A^2	magnetic constant
μ_{r}	-	-	relatice permeability
l_1	-	mm	tangential length of bridge 1
l_2	-	mm	tangential length of bridge 2
l_{m}	-	mm	length of the machine
θ_1	-	$^\circ\,(deg)$	barrier angle of barrier 1
θ_2	-	$^\circ\,(deg)$	barrier angle of barrier 2
d_{fp}	-	mm	flux path width
h_{m1}	1-5	mm	height of magnet 1
h_{m2}	1-5	mm	height of magnet 2
w_{m1}	2-6	mm	width of magnet 1
w_{m2}	2-9	mm	width of magnet 2
F_{Z}	-	N	centrifugal force
m	-	kg	mass
ω	-	rad/s	angular speed
r	-	mm	radius of rotating body
σ_{y}	330	MPa	elastic limit (yield strength)
d_{gap}	0.7	mm	air gap width
c	1-8	-	resolution factor for meshing
r_{Bridge}	0.1-0.4	mm	radius of bridge rounding
n	-	min^{-1}	speed

B. Parameterized rotor model

A main challenge of the construction of this type of machine is the amount of stray flux through the bridges between air gap and barrier. In table I all relevant parameters of the presented study are shown [10]. Fig. 2 shows a test model for the minimization of stray flux which is located at the lower barrier, barrier 2 [11], [12]. The iron in the bridges is saturated, what increases the reluctance of the material and lowers the stray flux in this area. In return the thin bridges d_1 and d_2 in Fig. 2 limit the maximum speed for the machine because of maximum allowable mechanical stress in the rotor. For this reason a compromise between higher torque with lower stray flux and higher speed with higher mechanical stability has to be found.

In Fig. 3 the flux density plot of one pole of a two-layer design is shown. On the right side of the second lower barrier, barrier 2, the flux flowing through the right tooth contributes to the saturation of the bridge, what is indicated by higher flux density in this area. On the left side the same saturation level of the bridge is present. This flux flows back to the lower magnet of barrier 2, which results in stray-flux. Therefore the bridges have to be designed in a long and thin shape. For this

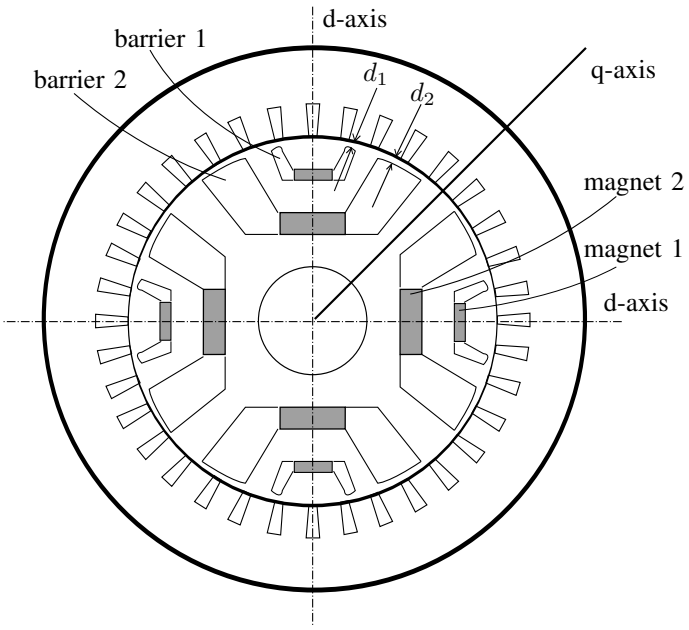

Figure 2. Example of a two-layer PMSynRM with assisting magnets in the center of the barrier. Testing case for very big second barrier with thin bridges. High synchronous and reluctance torque is achieved. Maximum allowed mechanical stress is exceeded in this example. Reference model for further calculations.

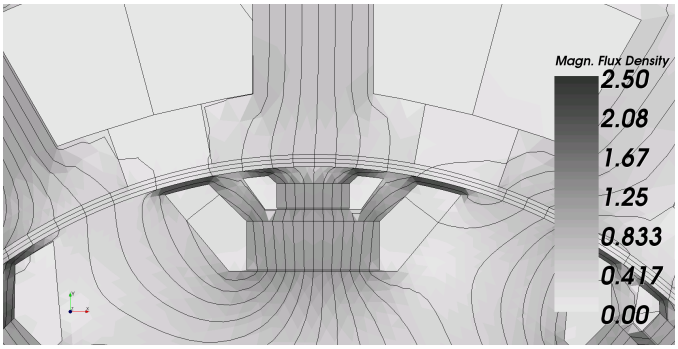

Figure 3. Simulation of magnetic flux density. Calculation with supplied current. Stray flux is shown on the left side of the second barrier. Saturation of the bridges is provided through the high magnetic flux density above 2.0 T.

reason the reluctance is maximized as shown in

$$R_{\mathrm{m}} = \frac{1}{\mu_0 \mu_{\mathrm{r}}} \frac{l_{1,2}}{l_{\mathrm{m}} \cdot d_{1,2}} \tag{2}$$

with permeability $\mu = \mu_0 \mu_{\mathrm{r}}$, length of the bridges l_1 and l_2 and the length of the machine l_{m} [13],[14]. A 2D model is applied for the simulation. Therefore, the length of the machine l_{m} can be neglected.

The flux path between the two layers of the barrier is important for the reluctance torque M_{rel}. To create a high reluctance torque in typical PMSM designs more than one layer is beneficial. Multiple layers give the possibility to form different flux paths and to design thinner magnets for each layer. In this paper exclusively two-layer constructions are considered, because this topology reveals the fundamental idea and understanding of this machine type [15].

A further design aspect is the length of the bridges. By

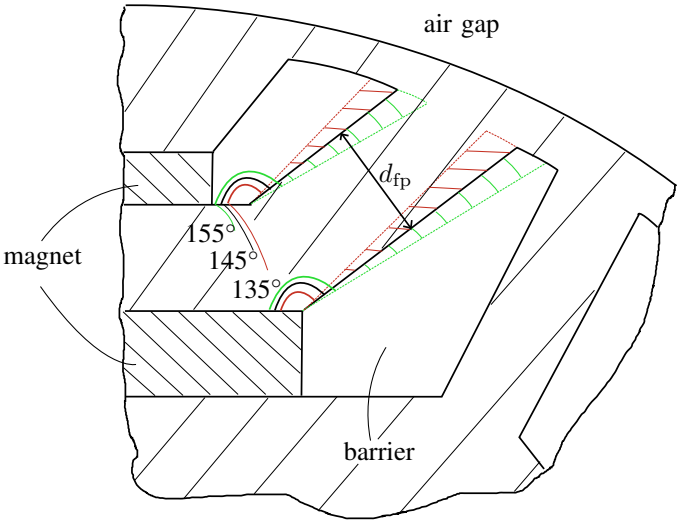

Figure 4. Variation of the length of the bridges by changing the barrier angles θ_1 and θ_2. Parallel flux path for optimal utilization.

variation of the barrier angles θ_1 and θ_2 on the side of the flux path of the barriers, the length of the bridges and the size of the barriers are changed. A study of different angle constellations for the first and the second barrier has been accomplished. Fig. 4 shows different barrier angles and the appropriate change in the barrier shape. Simulation results for synchronous, reluctance and total torque are shown in table II. A selection of values between 135° and 155° for both barrier angles has been calculated. In table II exemplarily three angles with results are presented. Constellations for different barrier angles in barrier 1 and barrier 2 result in a flux path getting thinner or wider to the outer side of the barrier. This results in a reduced available space for the barriers. The flux in this area is produced by the difference in the permanent magnet flux linkage Ψ_{PM} between the two magnets in the center of the barriers. Therefore a parallel construction of the flux path is recommended to obtain the design of the machine. The minimal flux path width in this area defines the maximum transfered flux. Table II shows, that smaller barrier angles result in higher synchronous torque and lower reluctance torque, while bigger barrier angels lead to smaller synchronous torque and higher reluctance torque. A beneficial constellation for total torque lies in between. Result of this analysis is a barrier angle of $\theta = 144°$. In this presented rotor design, the relevant component for improving the magnetic circuit is the size of barrier 2. Enlarging this barrier leads to a higher synchronous torque, because of lower stray flux. If the barrier is getting smaller, the q-flux through the flux path becomes higher and this results in higher reluctance torque.

C. Design rules for magnetic circuit

In the next section the remanence induction of the permanent magnets is variated to investigate their influence [16]. Fig. 5 shows the produced torque relating to the remanence induction of the permanent magnets. A concrete material is not assumed, but the range of values refers to typical rare-earth magnets like NdFeB or SmCo. The evaluation indicates,

Table II
TORQUE CALCULATION FOR DIFFERENT BARRIER ANGLES WITH PARALLEL FLUX PATH d_{fp}.

barrier angle	flux path	torque		
$\theta_{1,2}$	d_{fp}	M_{syn}	M_{rel}	M_{tot}
[°]	[mm]	[Nm]	[Nm]	[Nm]
135	2.47	4.37	2.25	5,73
145	2.74	4.11	2.54	5.77
155	2.93	3.70	2.70	5.57

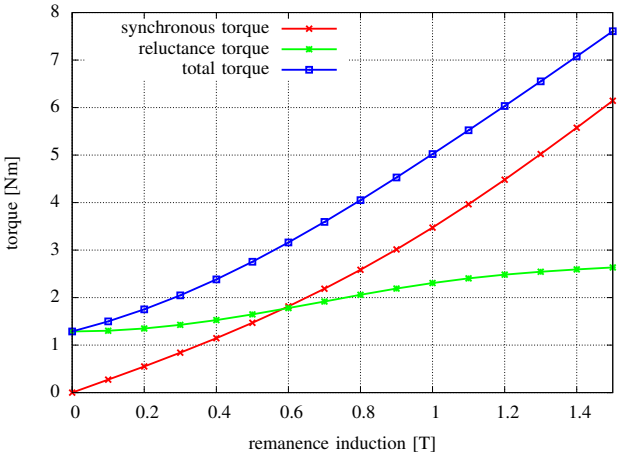

Figure 5. Synchronous, reluctance and total torque for different remanence inductions of the permanent magnets. The reluctance torque is indirectly influenced by the remanence induction because of better saturation of the bridges.

that the synchronous torque has a much higher dependency of magnet material than the reluctance torque. This correlation is expected, because only the synchronous torque is effected by the flux of permanent magnets. The increase of reluctance torque is explained by higher saturation of the bridges as consequence of higher flux. Therefore, the magnetic circuit is enhanced for the reluctance torque. As a conclusion follows that the selection of bridge widths is dependent on the interaction of synchronous and reluctance torque and thus both of them have to be taken into account for the analysis.

A further aspect, which is studied, is the variation of the air gap width d_{gap}. Fig. 6 shows the result of this analysis. The air gap width d_{gap} is variated between 0.5 mm and 1.0 mm. In all other simulations a constant air gap width of $d_{\mathrm{gap}} = 0.7$ mm is assumed. The variation shows, that smaller air gap width result in a higher total torque. The reluctance torque M_{rel} profits more by reducing the air gap width than the synchronous torque M_{syn}. This has to be considered for the relation between synchronous and reluctance torque and therefore, as explained in the previous section, for the design of the bridges.

Further design aspect arises from the variation of the geometric dimensions of the magnets [17]. Thereby the magnet height h_{m} and the magnet width w_{m} is changed and analyzed. The parameters are shown in Fig. 7. The size of the magnets corresponds with the produced magnetic flux linkage Ψ_{PM} and therefore with the stray flux in the bridges.

Table III shows the results of the evaluation for different magnet heights [18]. In the horizontal axis the magnet height h_{m1} of barrier 1 is variated, in the vertical axis the magnet height h_{m2} of barrier 2 is changed. According to the simplified design the barrier itself is changed appropriate to the magnet. The position of the barrier changes in radial direction, while the distance between barrier 1 and 2 and their barrier angles remain constant. In table III the synchronous torque is calculated relating to the sum of the cross-section area of the magnets. As a result of this analysis the thickness of the magnets has to be designed very small, to get an optimal utilization from the magnet material.

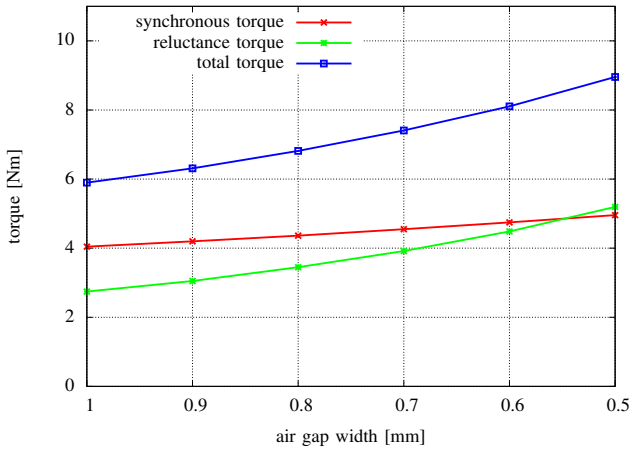

Figure 6. Variation of air gap width. Calculation of synchronous, reluctance and total torque. Influence of air gap width is higher for reluctance torque.

In table IV the width of the magnets w_{m} in the barriers is changed, while the position of the barriers and their shape is kept constant. As reference the design in Fig. 2 with smaller second barrier is chosen. The magnet height of both magnets is chosen to be the same. The highest utilization of magnet material is reached by maximizing the width w_{m2} of magnet 2 and minimizing the width w_{m1} of magnet 1. Because of equal magnet height the constellation $w_{\mathrm{m1}} = 2$ mm/$w_{\mathrm{m2}} = 6$ mm and $w_{\mathrm{m1}} = 6$ mm/$w_{\mathrm{m2}} = 2$ mm require the same amount of magnet material. The constellation with $w_{\mathrm{m2}} > w_{\mathrm{m1}}$ results in 25% higher synchronous torque. This can be explained by a more reduced stray flux due to a larger barrier 2. For very small magnet widths in barrier 2 the magnet flux of magnet 1 produces a high amount of stray flux, which circulates back through the flux path. This results in a worse magnet utilization in the first row for larger magnet widths of magnet 1. As conclusion for the geometric magnet dimensioning a small magnet height, but large magnet width is required. The size of the magnets always has to correspond to the size of the equivalent barrier, to minimize stray flux and increase the resulting torque.

As a result for the design of the magnetic circuit of a PM-SynRM thin and long bridges are recommended to minimize stray flux. There no variation in the shape of the barrier is performed, but a wide barrier close to the magnets and a thinner barrier in the sector of the bridges is advised. For the size of the barriers the height and the width of the permanent magnets have to be taken into account. A wider magnet results

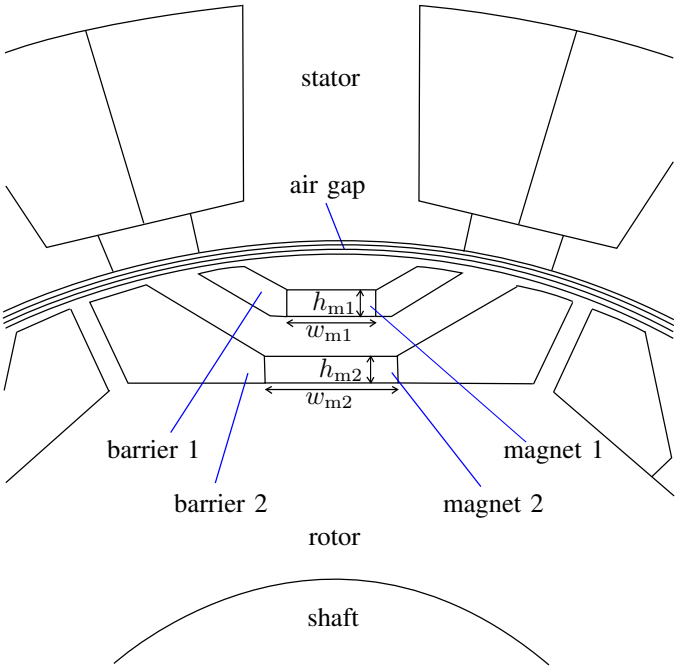

Figure 7. Variation of magnet height $h_{m1,m2}$ and magnet width $w_{m1,m2}$ of the permanent magnets. Variation of magnet height results in different position of the barriers. Flux path width d_{fp} remains constant for parameter study.

Table III
SYNCHRONOUS TORQUE PER MAGNET CROSS-SECTION FOR DIFFERENT MAGNET HEIGHT

synchronous torque M_{syn}/magnet cross-section [Nm/mm^2]					
height of magnet 2	height of magnet 1 1 mm	2 mm	3 mm	4 mm	5 mm
1 mm	0.2357	0.1730	0.1371	0.1133	0.0961
2 mm	0.1682	0.1369	0.1117	0.0952	0.0818
3 mm	0.1332	0.1110	0.0945	0.0816	0.0712
4 mm	0.1099	0.0934	0.0813	0.0705	0.0627
5 mm	0.0921	0.0801	0.0704	0.0623	0.0555

Table IV
SYNCHRONOUS TORQUE PER MAGNET CROSS-SECTION FOR DIFFERENT MAGNET WIDTH

synchronous torque M_{syn}/magnet cross-section [Nm/mm^2]					
width of magnet 2	width of magnet 1 2 mm	3 mm	4 mm	5 mm	6 mm
2 mm	0.2086	0.1938	0.1870	0.1871	0.1903
3 mm	0.2264	0.2103	0.2018	0.1987	0.1993
4 mm	0.2389	0.2226	0.2129	0.2080	0.2069
5 mm	0.2482	0.2323	0.2219	0.2159	0.2135
6 mm	0.2558	0.2404	0.2296	0.2228	0.2194
7 mm	0.2624	0.2476	0.2365	0.2291	0.2249
8 mm	0.2685	0.2542	0.2431	0.2352	0.2303
9 mm	0.2744	0.2606	0.2495	0.2411	0.2357

in more magnetic flux and hence the barrier needs to be larger to keep the stray flux low. The space for barrier 2 is larger than for barrier 1 and thus also the second magnet, magnet 2, is slightly larger than magnet 1. After the magnetic design of the machine, a mechanical evaluation is performed in the next section.

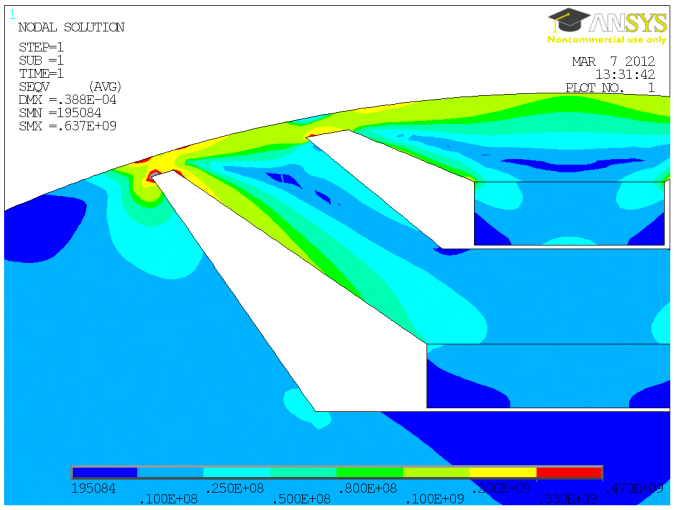

Figure 8. Local mechanical stress for an extract of a half pole. Barriers are designed with simplified geometry, consisting of barrier angles, sharp corners and magnets with rectangular cross-section. Small elements in the mesh, especially in the corners of the barrier are needed. Calculation results are interpreted in detail in this section.

III. MECHANICAL EVALUATION

Besides the electro-magnetic construction of the machine, a mechanical evaluation is necessary [19]. Main objective is the calculation of operating centrifugal force in the rotor which generates a local stress in the bridges of the machine. The centrifugal force can be described by

$$F_Z = m \cdot \omega^2 \cdot r \tag{3}$$

with mass m, angular speed ω and radius r. The angular speed ω is proportional to the speed n and the centrifugal force F_Z increases with the square of angular speed ω, which leads to a sharp increase of mechanical stress for higher speed values.

Based on typical stress-strain curves the elastic limit (yield strength) σ_y of the material is chosen as reference for the maximum appearing stress in the rotor [20]. To determine the maximum speed of the machine the overspeed will be concerned. A variation of different bridge widths of the two corresponding bridges is performed. The width of the bridges of barrier 1 and barrier 2 is changed from $d_{1,2} = 0.2$ mm to $d_{1,2} = 2.0$ mm. This design range has been chosen to provide a wide overview of the concept. To describe the mechanical stability the stress is analyzed by numerical simulation.

The simulated mechanical stress in Fig. 8 shows local hot spots in the area of the bridges. Because of the higher amount of material above barrier 2 in comparison to barrier 1, the calculated stress at the bridges of barrier 2 is higher. This results in a smaller design of the bridge width of barrier 1 to reduce stray flux at this location. The position of the maximum stress is always arranged in the corner of the second bridge on the outer side of the barrier. This concentration of stress is known as the notching effect and will be discussed later in this section. To provide an appropriate calculation of the stress a mesh with small elements is necessary. The bridges have a maximum mesh size of five layers.

Table V
ANALYSIS OF STRESS IN THE ROTOR FOR DIFFERENT MESHING.

resolution factor c	8	6	4	3	2	1
max. stress [MPa]	490	522	625	833	805	945
min. bridge stress	218	232	139	185	179	210
max. bridge stress	272	290	209	278	269	315

Table VI
MECHANICAL STRESS IN THE ROTOR. ROUNDING OF THE CORNERS OF THE BRIDGES. SIMULATION AND ANALYSIS FOR DIFFERENT SPEED VALUES OF THE MACHINE AND RADII OF THE ROUNDING.

Radius	$9000\,\mathrm{min}^{-1}$		$18000\,\mathrm{min}^{-1}$	
[mm]	stress [MPa]		stress [MPa]	
	max	analysis	max	analysis
0.1	169	50	676	200
0.2	167	48	667	189
0.3	146	48	585	171
0.4	136	40	545	150

Because of the chosen geometry the calculation in the peaked corner of the barrier results in an excessive mechanical stress value. This can be explained by the notching effect. In reality this point is support by the ambient material, which causes a local elastic expansion of the material. A study for different mesh resolutions has been performed and is shown in table V. The resolution factor c describes how small the elements of the mesh have been chosen. The maximum mechanical stress describes the excessive values in the peaked corner of the barrier. Minimum and maximum stress value in the bridges considering the notching effect are evaluated. By refining the mesh the appearing notching effect is reduced, which improves the accuracy of the resulting stress calculation. As reference for further calculations the maximum mechanical stress value by neglecting the calculated excessive value in the corner is used. A high resolution factor c with fine mesh is recommended.

Fig. 9 shows the improvement of the barrier geometry at the bridge by rounding the corner [21]. r_{Bridge} is the radius of this rounding, $d_{1,2}$ describes the bridge width. On the one hand by rounding the corner the notching effect and thus the local maximum stress is reduced. On the other hand the rounding enlarges the width of the bridge at the corner, which increases the stray flux and thereby reduces the produced torque for this constellation. In table VI the local stress is described for different radii of the rounding r_{bridge}. The table shows the maximum calculated value without considering the notching effect in the column labeled with 'max'. In the column labeled with 'analysis' the previously described maximum bridge value is concerned. The simulated maximum stress can be reduced by 20-25% by varying the rounding radius r_{bridge} from 0.1 mm to 0.4 mm. The analysis results have a maximum of 200 MPa at 0.1 mm radius and $18000\,\mathrm{min}^{-1}$ overspeed. A typical yield strength is $\sigma_{\mathrm{y}} = 330\,\mathrm{MPa}$ und therefore the simulation results are uncritical regarding the mechanical stability. The appropriate electro-magnetic simulations with different radii of the rounding show a negligible increase of stray flux caused by the higher bridge cross-section and because of that the reduction of synchronous torque M_{syn} was neglected [22].

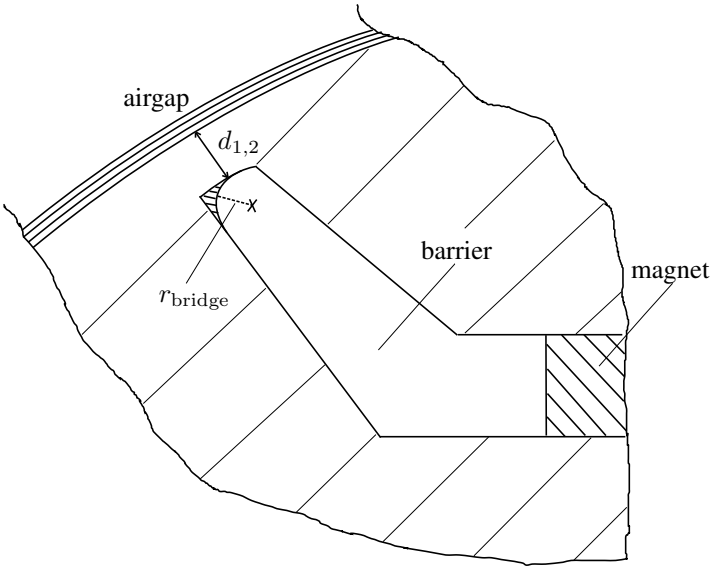

Figure 9. Rounding of barrier corners to counteract notching effects. Different radii for the rounding r_{Bridge} between 0.1 mm and 0.4 mm are concerned to reduce the local stress in this area.

Table VII
VARIATION OF THE BRIDGE WIDTH FOR BOTH BRIDGES SIMULTANEOUSLY. CALCULATION OF SYNCHRONOUS, RELUCTANCE AND TOTAL TORQUE.

bridge width $d_{1,2}$ [mm]	0.2	0.6	0.8	1.0	2.0
synchronous torque M_{syn} [Nm]	4.25	3.39	3.00	2.63	1.19
reluctance torque M_{rel} [Nm]	2.82	2.44	2.27	2.09	1.19
total torque M [Nm]	6.14	5.08	4.59	4.12	2.10

The next step in the design of the PMSynRM is the combination of electro-magnetic and mechanical evaluation to receive an optimal design through the design factor k. Apart from calculations of the mechanical stress the corresponding maximum speed for every constellation has to be considered, what will be presented in the next section.

IV. COMPARISON OF ELECTRO-MAGNETIC AND MECHANICAL EVALUATION

The agreement between stray-flux and stability, being described by the selection of appropriate bridges, is transformed to the relation between higher torque or speed, that can be optimized by an objective function. This factor combines resulting speed and torque to evaluate a value related to the power for the design of the machine.

In the evaluation the bridges are varied in both barriers simultaneously. Table VII shows a selection of bridge widths $d_{1,2}$ and the calculated synchronous, reluctance and total torque of the machine. The corresponding data is pictured in detail in Fig. 10. Because of higher stray flux the synchronous torque M_{syn} decreases with higher bridge width. A higher bridge width also reduces the reluctance torque M_{rel}, but the decrease is less than that one of the synchronous torque. This means, that the synchronous part of the PMSynRM is more sensitive for bridge width changes than the reluctance part.

The maximum stress in the bridges is analyzed for $n = 9000\,\mathrm{min}^{-1}$ and $n = 18000\,\mathrm{min}^{-1}$ for the selection of

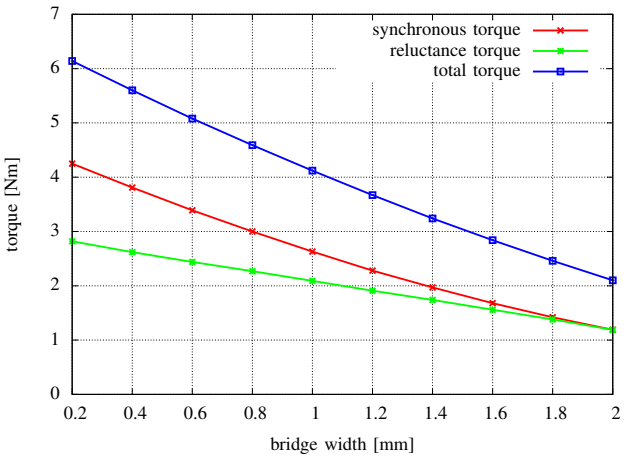

Figure 10. Synchronous, reluctance and total torque as a function of bridge width $d_{1,2}$. Bridge width is changed for both bridges simultaneously. Synchronous torque is more sensitive towards variations in bridge widths.

Table VIII
MAXIMUM MECHANICAL STRESS [MPA] WITH SPEED n=18000 MIN^{-1}

bridge 1	bridge 2 [mm]					
[mm]	0.4	0.6	0.8	1.0	1.2	1.4
0.4	-	-	432	433	422	-
0.6	-	458	291	285	303	252
0.8	584	402	318	292	253	236
1.0	-	422	321	296	245	-
1.2	-	401	336	-	-	-

Table IX
MAXIMUM MECHANICAL STRESS [MPA] WITH SPEED n=9000 MIN^{-1}

bridge 1	bridge 2 [mm]					
[mm]	0.4	0.6	0.8	1.0	1.2	1.4
0.4	-	-	108	107	105	-
0.6	-	114	73	71	76	63
0.8	141	102	79	73	63	59
1.0	-	106	80	74	61	-
1.2	-	100	84	-	-	-

bridge widths $d_{1,2}$ shown in table VIII and table IX. Calculations at $n = 18000\,\text{min}^{-1}$ in table VIII for $d_1 = 0.4\,\text{mm}$ or smaller and $d_2 = 0.6\,\text{mm}$ or smaller cause a maximum local stress in the bridges higher than 330 MPa and hence will be omitted from the possible constellations. Higher bridge widths $d_{1,2}$ are uncritical for mechanical stress. For lower speed $n = 9000\,\text{min}^{-1}$, shown in table IX, all bridge width constellations are valid.

In consideration of the maximum allowed local stress in the bridges, a corresponding speed can be calculated with the correlation $F_Z \propto n^2$ as described in (3). The simulation for a given speed n, resulting in the maximum local stress at the bridges, is interpolated for different values of speed. Hence, the equivalent speed for the allowed yield strength $\sigma_y = 330\,\text{MPa}$ is calculated. These results are shown in table X and dependent on the bridge widths d_1 and d_2. An extract for relevant values is obtained. On the vertical axis the variations of the bridge width of barrier 1 are applied, on the horizontal axis the variations of the bridge

Table X
CALCULATION OF MAXIMUM ALLOWED SPEED BY INDEPENDENT ADJUST OF BRIDGE WIDTHS.

maximum speed [min^{-1}]	yield strength σ_y: 330 MPa					
bridge 1	bridge 2 [mm]					
[mm]	0.4	0.6	0.8	1.0	1.2	1.4
0.4	-	-	15732	15727	15922	-
0.6	-	15285	19170	19367	19786	20598
0.8	13606	16296	18335	19135	20552	21285
1.0	-	15913	18250	19006	20884	-
1.2	-	16331	17839	-	-	-

width of barrier 2 are shown. For higher bridge widths the allowed speed is higher. The variation of $d_1 = 0.6\,\text{mm}$ shows a permanently increasing maximum speed n between $15000\,\text{min}^{-1}$ and $20000\,\text{min}^{-1}$. In this case the limiting bridge width for the stability of the rotor is the bridge width of the second barrier d_2. However, in the variation of $d_2 = 0.6\,\text{mm}$ the allowed maximum speed n is between $15000\,\text{min}^{-1}$ and $16000\,\text{min}^{-1}$. Table X shows, that choosing the bridge widths has to be done for every barrier independently to reach the optimal design. The results are approximations for an early design of the machine.

Adapted from the electro-magnetic calculation of maximum total torque for different constellations of bridge widths $d_{1,2}$ and the mechanical evaluation with maximum permitted speed based on the appearing stress the design factor k can be calculated. By multiplying torque and speed in this combination the design factor k results in

$$k = n_{\max} \cdot M_{\max} \tag{4}$$

and represents the result of the objective function. In this case the speed $n_{\max}$ is a matrix for different bridge widths $d_{1,2}$, which are arranged vertical for barrier 1 and horizontal for barrier 2. The speed is interpolated from maximum local mechanical stress in the bridges, which is analyzed in consideration of meshing resolution and notching effects. The appropriate total torque is considered for a synchronous part M_{syn} and a reluctance part M_{rel}. It is simulated for an operation point without field weakening at $3000\,\text{min}^{-1}$. The magnetic circuit is improved by adjusting the barrier angles, magnet dimensions and air gap width. Therefore the design factor k has the unit Watt but does not describe the existing power in the machine, because speed and torque are derived from different operating points of the machine.

In table XI the final results for the selection of evaluations are shown. A maximum of the design factor k is reached for the bridge width constellation of $d_1 = 0.6\,\text{mm}$ and $d_2 = 0.8\,\text{mm}$. For larger bridge widths higher maximum speed is possible but also the total achievable torque is lower, because of higher stray flux through the bridges. The design factor k shows, that in this case the benefit of higher speed does not compensate the loss in producible torque. On the other side for smaller bridge widths $d_{1,2}$ the maximum speed is decreased rapidly but the benefit in produced torque by lower stray flux does not rise in the same dimension.

As a conclusion of the previous provided considerations the design factor k is applied to obtain beneficial constellation for

Table XI
CALCULATION OF DESIGN FACTOR k.

design factor k [W]						
bridge 1	bridge 2 [mm]					
[mm]	0.4	0.6	0.8	1.0	1.2	1.4
0.4	-	-	79110	75028	72136	-
0.6	-	77638	91854	87539	80117	82922
0.8	70728	79601	84081	82314	82874	80412
1.0	-	75114	80509	78226	80063	-
1.2	-	74898	76143	-	-	-

the bridge widths by analyzing electro-magnetic and mechanical aspects to find an appropriate compromise.

V. CONCLUSIONS

Designing the geometry of electrical machines is an important challenge at the construction of the machine. The agreement between high electro-magnetic performance and mechanical stability has to be taken into account. Especially the design of a permanent magnet synchronous reluctance machine (PMSynRM) with a complex rotor geometry requires a detailed study for the width of the bridges. This paper gives an instruction on how to analyze this problem, which can be used for constructing and designing a PMSynRM. Numerical simulations and calculations enable the transformation into typical machine parameters (torque and speed) which are summarized in an objective function for the evaluation of the machine. This objective function provides a design factor for selecting the beneficial constellation of bridge widths. The total torque has been calculated with respect to the magnetic circuit by independent variations of bridge widths and barrier angles. The design has been performed to increase synchronous- and reluctance torque and an beneficial compromise is determined. The mechanical evaluation provides a local mechanical stress result considering of simulation accurateness and notching effects. The maximum reachable speed of the machine is calculated for a parameter variation of the bridge widths. The design factor is established to give a procedure for constructing the machine. For this example of a PMSynRM a beneficial bridge width for the upper bridge of the first barrier and the lower bridge of the second barrier is obtained.

REFERENCES

[1] N. Bianchi, S. Bolognani, D. Bon, and M. Dai Pre, "Rotor flux-barrier design for torque ripple reduction in synchronous reluctance and PM-Assisted synchronous reluctance motors," *IEEE Transactions on Industry Applications*, vol. 45, no. 3, pp. 921–928, Jun. 2009.

[2] S.-Y. Kwak, J.-K. Kim, and H.-K. Jung, "Inductance and torque characteristic analysis of multi-layer buried magnet synchronous machine," in *Sixth International Conference on Electrical Machines and Systems, 2003. ICEMS 2003*, vol. 1. IEEE, Nov. 2003, pp. 104– 107 vol.1.

[3] I. Boldea, L. Tutelea, and C. I. Pitic, "PM-assisted reluctance synchronous motor/generator (PM-RSM) for mild hybrid vehicles: electromagnetic design," *IEEE Transactions on Industry Applications*, vol. 40, no. 2, pp. 492– 498, Apr. 2004.

[4] P. Niazi, H. A. Toliyat, D.-H. Cheong, and J.-C. Kim, "A low-cost and efficient permanent-magnet-assisted synchronous reluctance motor drive," *IEEE Transactions on Industry Applications*, vol. 43, no. 2, pp. 542–550, Apr. 2007.

[5] N. Bianchi, S. Bolognani, and B. J. Chalmers, "Salient-rotor PM synchronous motors for an extended flux-weakening operation range," *IEEE Transactions on Industry Applications*, vol. 36, no. 4, pp. 1118–1125, Aug. 2000.

[6] A. S. Ogunjuyigbe, A. A. Jimoh, D. V. Nicolae, and E. S. Obe, "Analysis of synchronous reluctance machine with magnetically coupled three-phase windings and reactive power compensation," *IET Electric Power Applications*, vol. 4, no. 4, pp. 291–303, Apr. 2010.

[7] D. Schroeder, *Elektrische Antriebe - Regelung von Antriebssystemen*. Springer Verlag, 2001.

[8] S. Y. Kwak, J. K. Kim, and H. K. Jung, "Characteristic analysis of multilayer-buried magnet synchronous motor using fixed permeability method," *IEEE Transactions on Energy Conversion*, vol. 20, no. 3, pp. 549– 555, Sep. 2005.

[9] I. Boldea, *Reluctance Synchronous Machines and Drives*. Clarendon Press, Oxford, 1996.

[10] A. M. El-Refaie and T. M. Jahns, "Comparison of synchronous PM machine types for wide constant-power speed range operation," in *Industry Applications Conference, 2005. Fourtieth IAS Annual Meeting. Conference Record of the 2005*, vol. 2. IEEE, Oct. 2005, pp. 1015–1022 Vol. 2.

[11] N. Bianchi and S. Bolognani, "Interior PM synchronous motor for high performance applications," in *Proceedings of the Power Conversion Conference, 2002. PCC Osaka 2002*, vol. 1. IEEE, 2002, pp. 148–153 vol.1.

[12] D. Zarko, "A systematic approach to optimized design of permanent magnet motors with reduced torque pulsation," Ph.D. dissertation, University of Wisconsin-Madison, 2004.

[13] D. Hanselman, *Brushless Permanent-Magnet Motor Design*. McGraw-Hill Inc., 1994.

[14] L. Song, D. Jiang, S. Cui, and S. Sheng, "Reluctance torque analysis and reactance calculation of IPM for HEVs based on FEM," in *2010 IEEE Vehicle Power and Propulsion Conference (VPPC)*. IEEE, Sep. 2010, pp. 1–4.

[15] G.-S. Choi, J.-Y. Lee, K.-N. Park, and S.-C. Hahn, "Characteristic analysis of high-speed interior permanent magnet synchronous motor," in *International Conference on Electrical Machines and Systems, 2009. ICEMS 2009*. IEEE, Nov. 2009, pp. 1–4.

[16] H. Murakami, Y. Honda, Y. Sadanaga, Y. Ikkai, S. Morimoto, and Y. Takeda, "Optimum design of highly efficient magnet assisted reluctance motor," in *Conference Record of the 2001 IEEE Industry Applications Conference, 2001. Thirty-Sixth IAS Annual Meeting*, vol. 4. IEEE, Oct. 2001, pp. 2296–2301 vol.4.

[17] K. Khan, M. Leksell, and O. Wallmark, "Design aspects on magnet placement in permanent-magnet assisted synchronous reluctance machines," in *5th IET International Conference on Power Electronics, Machines and Drives (PEMD 2010)*. IET, Apr. 2010, pp. 1–5.

[18] T. Tokuda, M. Sanada, and S. Morimoto, "Influence of rotor structure on performance of permanent magnet assisted synchronous reluctance motor," in *International Conference on Electrical Machines and Systems, 2009. ICEMS 2009*. IEEE, Nov. 2009, pp. 1–6.

[19] S.-M. Cho, J.-K. Kim, H.-K. Jung, and C.-G. Lee, "Stress and thermal analysis coupled with field analysis of multilayer buried magnet synchronous machine with a wide speed range," *IEEE Transactions on Magnetics*, vol. 41, no. 5, pp. 1632– 1635, May 2005.

[20] A. Binder, T. Schneider, and M. Klohr, "Fixation of buried and surface-mounted magnets in high-speed permanent-magnet synchronous machines," *IEEE Transactions on Industry Applications*, vol. 42, no. 4, pp. 1031–1037, Aug. 2006.

[21] Y. Honda, T. Higaki, S. Morimoto, and Y. Takeda, "Rotor design optimisation of a multi-layer interior permanent-magnet synchronous motor," *Electric Power Applications, IEE Proceedings* -, vol. 145, no. 2, pp. 119–124, Mar. 1998.

[22] K. Khan, S. Haghbin, M. Leksell, and O. Wallmark, "Design and performance analysis of a permanent-magnet assisted synchronous reluctance machine for an integrated charger application," in *2010 XIX International Conference on Electrical Machines (ICEM)*. IEEE, Sep. 2010, pp. 1–6.